Solution Deposition of a Bournonite $CuPbSbS_3$ Semiconductor Thin Film from the Dissolution of Bulk Materials with a Thiol-Amine Solvent Mixture

Kristopher M. Koskela, Brent C. Melot, and Richard L. Brutchey*

Department of Chemistry, University of Southern California, Los Angeles, CA 90089, United States

ABSTRACT: There is considerable interest in the exploration of new solar absorbers that are environmentally stable, absorb through the visible, and possess a polar crystal structure. Bournonite $CuPbSbS_3$ is a naturally occurring sulfosalt mineral that crystallizes in the non-centrosymmetric $Pmn2_1$ space group and possesses an optimal band gap for single junction solar cells; however, the synthetic literature on this quaternary semiconductor is sparse and it has yet to be deposited and studied as a thin film. Here we describe the ability of a binary thiol-amine solvent mixture to dissolve the bulk bournonite mineral as well as inexpensive bulk CuO, PbO, and Sb_2S_3 precursors at room temperature and ambient pressure to generate an ink. The synthetic compound ink derived from the dissolution of the bulk binary precursors in the right stoichiometric ratios yields phase-pure thin films of $CuPbSbS_3$ upon solution deposition and annealing. The resulting semiconductor thin films possess a direct optical band gap of 1.24 eV, an absorption coefficient ~10^5 cm^{-1} through the visible, mobilities of 0.01-2.4 cm^2 $(V•s)^{-1}$, and carrier concentrations of 10^{18} – 10^{20} cm^{-3}. These favorable optoelectronic properties suggest $CuPbSbS_3$ thin films are excellent candidates for solar absorbers.

INTRODUCTION

The discovery of hybrid lead halide perovskite solar absorbers has garnered massive attention because of their high power conversion efficiencies in solar cells, which are now in excess of 23%, in addition to their ability to be inexpensively solution processed.[1-3] The high power conversion efficiencies realized for these hybrid lead halide perovskites can be attributed, in part, to their long minority carrier lifetimes (~280 ns)[4] and diffusion lengths (up to ~175 μm).[5] It has been suggested that the presence of polar domains within $MAPbI_3$ (MA = methylammonium) help facilitate the low recombination rates and subsequent spatial separation of charge carriers.[6] Unfortunately, devices based on hybrid lead halide perovskites suffer from environmental instability issues and short device lifetimes (under ambient conditions) because of moisture sensitivity.[7] As such, there is interest in the discovery of new thin film solar absorber candidates that possess greater environmental stability.

In a recent study by Wallace et al., the authors screened nearly 200 naturally occurring multinary minerals to identify dark colored materials (translating to suitable band gaps E_g = 1.0-1.7 eV) that also assume crystal structures with a polar point group.[8] By screening for naturally occurring minerals, the resulting materials possess thermodynamic stability and should not have the same environmental instability issues inherent to hybrid lead halide perovskites. Polar structures may decrease exciton binding energies and reduce recombination rates in the material; moreover, a polar crystal structure may minimize the chance of dipole-disallowed transitions and a corresponding reduction in oscillator strength at the absorption onset for direct band gap materials.[8-10] One of the resulting materials that satisfied the selection criteria out of the naturally occurring multinary minerals that were screened was bournonite $CuPbSbS_3$. Bournonite $CuPbSbS_3$ is a sulfosalt mineral (Strunz 2.GA.50), which crystallizes in the orthorhombic $Pmn2_1$ space group with experimentally reported band gaps from 1.20 eV[11] to 1.31 eV[12] that are optimal for single junction solar cells. Structurally, bournonite is derivative of the naturally occurring stibnite (Sb_2S_3) structure, where the

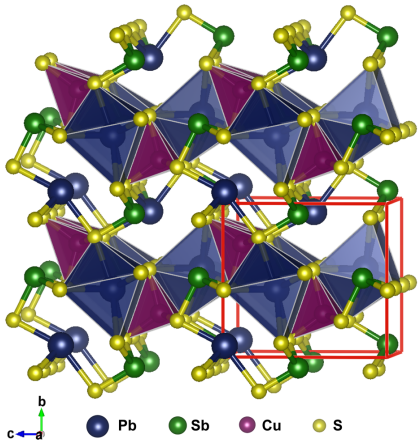

Figure 1. Crystal structure of bournonite $CuPbSbS_3$ (space group $Pmn2_1$).

Pb^{2+} cations alternately occupy the Sb^{3+} positions, and Cu^{+} occupies tetrahedral holes to charge compensate (**Figure 1**).[8,13] The synthetic literature on $CuPbSbS_3$ is sparse, with only a handful of solid-state syntheses[11,14,15] and one solvothermal synthesis having been reported thusfar.[12] The solid-state syntheses of $CuPbSbS_3$ are energy intensive – requiring annealing temperatures >550 °C and annealing times >30 d – and result in bulk material with persistent binary PbS impurities.[14,15] To date, this material has not been deposited or studied in thin film form, which is needed for future application work.

With respect to thin film deposition, solution methods (e.g., spin coating, spray coating, etc.) have the potential to significantly reduce deposition costs over more traditional and energy intensive physical vapor deposition methods.[16,17] Solution processable molecular inks are known to give excellent film homogeneity;[18-20] however, the dissolution of inexpensive bulk material precursors is significantly hampered by the general insolubility of these materials in typical solvents. In response, we developed an "alkahest" solvent system that utilizes a binary mixture of short chain thiols and amines that is capable of dissolving over 100 bulk materials, including bulk metals, metal chalcogenides, and metal oxides.[21-27] The resulting inks return phase-pure chalcogenide thin films upon solution deposition and mild annealing through a dissolve and recover approach, making it potentially suitable for large-scale solution processing.[27] Indeed, thiol-amine inks have been effectively utilized for the solution deposition of small area chalcopyrite and kesterite-based solar cells with excellent power conversion efficiencies.[28-30] The relatively mild conditions required for thin film deposition from the thiol-amine inks is particularly promising for sulfosalt materials in order to minimize reaction with back contact materials, such as Mo, in thin film solar cell architectures.[31] Herein, we are the first to demonstrate the deposition of bournonite $CuPbSbS_3$ thin films. The viability of the resulting solution-processed thin films as absorber layers is assessed with a combination of optical and electrical measurements.

EXPERIMENTAL SECTION

General Considerations. All materials were used as received. 1,2-Ethylenediamine (en, 99.5%), copper(II) oxide (CuO, 99.99%), lead(II) oxide (PbO, 99.999%), and antimony(III) sulfide (Sb_2S_3, 99.995%) were purchased from Sigma Aldrich. 1,2-Ethanedithiol (EDT, 98+%) was purchased from Alfa Aesar. Copper, lead, and antimony ICP standards (1000 ppm in 2% aqueous nitric acid) were purchased from Perkin Elmer. A natural sample of the mineral bournonite (catalog no. 67450; mined from Chihuahua, Mexico) was obtained from the Natural History Museum of Los Angeles County.

Synthetic Ink Preparation. For the preparation of a typical ink, 9.9 mg (0.124 mmol) CuO, 25.9 mg (0.116 mmol) PbO, and 22.5 mg (0.066 mmol) Sb_2S_3 were stirred together in a mixture of 0.2 mL EDT and 0.8 mL en for 12 h at 25 °C under ambient conditions. Full dissolution occurred, resulting in an optically clear, free-flowing orange-brown solution. For spin coating, a 2× concentrated ink was formulated using 9.9 mg (0.124 mmol) CuO, 25.9 mg (0.116 mmol) PbO, and 22.5 mg (0.066 mmol) Sb_2S_3 in a mixture of 0.1 mL EDT and 0.4 mL en, likewise resulting in an optically clear, free-flowing orange-brown solution. If the solvents solidified upon the initial addition to the bulk precursors, a heat gun was used to solubilize the ink.

Thin Film Deposition. Films were spin coated on 1 cm^2 borosilicate glass substrates that were cleaned by sequential bath sonication in acetone, isopropyl alcohol, and deionized water (20 min each), followed by drying under flowing nitrogen. The 2× concentrated ink was spin coated onto the substrate using a Laurell Technologies Corporation WS400Ez-6NPPLITE single-wafer spin processor at 3000 rpm for 1 min under a flowing nitrogen atmosphere. In between coats, the films were annealed at 390 °C for 10 min in a temperature-controlled aluminum annealing chamber under flowing nitrogen and allowed to cool naturally to room temperature before the next coat of ink was applied. After 3 coats, the films were annealed to 450 °C in a tube furnace under flowing nitrogen for 20 min and allowed to naturally cool to room temperature. Films were exposed to air between coats.

Natural Bournonite Ink Preparation. 60 mg of the natural bournonite sample was crushed with an agate mortar and pestle and subsequently stirred in a mixture of 0.2 mL EDT and 0.8 mL en for 12 h at 25 °C. This resulted in full dissolution giving an optically clear, orange-brown solution. The ink was drop cast onto a borosilicate glass substrate and subsequently annealed to 350 °C in a temperature-controlled aluminum annealing chamber under flowing nitrogen for 20 min before cooling to room temperature. The bulk material was then annealed to 450 °C in a tube furnace under flowing nitrogen for 96 h and allowed to naturally cool to room temperature.

Structural and Optical Characterization. Powder X-ray diffraction (XRD) patterns were collected using a Rigaku Miniflex600 operated at 40 mA and 35 kV, in the 2θ range of 10-70° using Cu *K*α radiation (λ = 1.5406 Å). For powder diffraction studies, inks were drop cast on a glass slide and dried to 330-390 °C in an aluminum annealing chamber under flowing nitrogen. The powders were collected from the glass slide using a razor blade and crushed in an agate mortar and pestle before being put into alumina crucible for annealing at elevated temperatures in a tube furnace under flowing nitrogen. For structural refinements, the step size and collection time were 0.05° and 3 s $step^{-1}$, respectively. All patterns were recorded under ambient conditions. Rietveld refinements were carried out using the General Structure Analysis System (GSAS) software package. The following parameters were refined: (1) scale factor, (2) background (modeled using a shifted Chebyschev polynomial function), (3) peak shape (modeled using a modified Thompson-Cox-Hastings pseudo-Voigt function), (4) lattice constants (*a*, *b*, *c*), (5) fractional atomic coordinates of the Cu, Pb, Sb, and S

atoms constrained by the site symmetry, (6) preferred orientation using a spherical harmonic model, and (7) isotropic thermal parameters for each chemical species. The R_{wp} and χ^2 indicators were employed to assess the quality of the refined structural models. UV-vis-NIR transmittance spectroscopy was performed on a Perkin Elmer Lambda 950 equipped with a 150-mm integrating sphere. The thin film on glass was placed in front of the integrating sphere.

Property Measurements. Temperature- and magnetic field-dependent electrical conductivity measurements were performed on thin films of $CuPbSbS_3$ (ranging in median thickness from 562-570 nm) on a 1 cm^2 borosilicate glass substrate. The film was argon sputtered with a Cressington Sputter Coater 108 (Liverpool, UK) for 90 s to remove the surface oxide layer that arises from exposing the sample to air in order to establish better ohmic contacts. Copper leads were immediately affixed at each corner of the thin film using a conductive silver paint (Ted Pella, Inc.). The sample was mounted in a Quantum Design Physical Properties Measurement System (PPMS), which was used to control the sample temperature and apply a magnetic field of 10000 Oe. Data were collected using a Keithley 2182A nanovoltmeter and a Keithley 6220 current source, controlled by a Keithley 7065 Hall effect card.

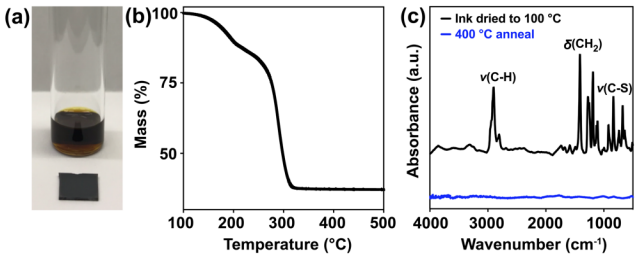

Figure 2. (a) Photograph of the synthetic ink prepared from the dissolution of bulk CuO, PbO, and Sb_2S_3 powders in a 1:4 (vol/vol) mixture of EDT and en alongside a 1 cm^2 $CuPbSbS_3$ thin film. (b) TGA trace of the dried ink showing an endpoint of decomposition < 350 °C. (c) FT-IR spectra of the ink dried at 100 °C under vacuum and annealed to 400 °C under flowing nitrogen.

RESULTS AND DISCUSSION

Ink Preparation and Conversion. Bulk powders of CuO, PbO, and Sb_2S_3 (1.0:1.0:0.53 mol/mol/mol, respectively) were mixed as solid precursors to formulate the compound $CuPbSbS_3$ ink by dissolution in a 1:4 (vol/vol) binary solvent system comprised of ethanedithiol (EDT) and ethylenediamine (en), respectively, giving an overall concentration of ~60 mg of total solids per mL of solvent. In this solvent mixture of 1:4 (vol/vol) EDT and en, CuO, PbO, and Sb_2S_3 have approximate room temperature and ambient pressure solubility limits of 10-15, 20-30, and 25-30 wt%, respectively. It has been shown that bulk oxide precursors fully dissolve, with the likely by-product being water, and transform into the corresponding sulfide with the thiol acting as a sulfur source.[32] All of the ink components were added together and stirred at room temperature and ambient pressure, giving full dissolution in < 20 min to yield an optically clear, free-flowing orange-brown solution (**Figure 2a**). The ink

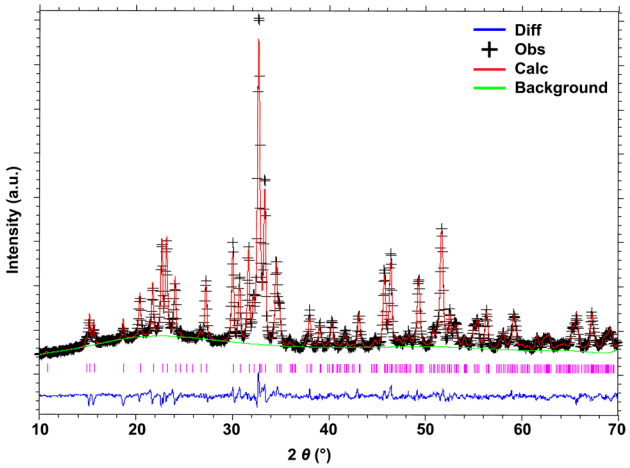

Figure 3. Powder XRD pattern of phase-pure $CuPbSbS_3$ drop-cast from the ink and annealed to 450 °C, with the results from a Rietveld refinement to the orthorhombic $Pmn2_1$ structure. Cross marks (+) represent experimental data points and pink tick marks represent individual reflections of the bournonite structure with the difference pattern shown below in blue. (λ = 1.5406 Å; R_{WP} = 4.96%; χ^2 = 2.48)

was stable (i.e., free from precipitates and color change) both in air and under inert atmosphere for several weeks at room temperature.

Thermogravimetric analysis (TGA) indicated an endpoint of decomposition of the dried ink well before 350 °C (**Figure 2b**), while the associated FT-IR bands attributable to organic species from the thiol-amine solvent system disappear upon heating the dried ink from 100 to 400 °C, corroborating the thermal volatilization and decomposition of organic content (**Figure 2c**). The strongest IR bands in the spectrum of the ink dried to 100 °C correspond to EDT (i.e., 2970 cm^{-1} ν(C–H) stretch, 2930 cm^{-1} ν(C–H) stretch, and 1430 cm^{-1} $\delta(CH_2)$ bend).[33] The sulfhydryl ν(S–H) stretching band is noticeably absent from the FT-IR spectrum of the dried ink, which is in agreement with previous reports that showed complete deprotonation of EDT in thiol-amine inks.[20,21] This is also confirmed by the shift of the ν(C–S) stretch from 699 cm^{-1} for protonated EDT to 675 cm^{-1} in the ink.[26] No significant IR bands were observed above 3000 cm^{-1}, where the ν(N–H) stretches are expected, indicating that en may be mostly absent in the ink after drying at 100 °C.

While the TGA and FT-IR data suggest that annealing to temperatures between 350-400 °C is sufficient to remove the volatile organic content and decomposition products from the ink, powder X-ray diffraction (XRD) studies revealed that higher annealing temperatures are required to recover phase-pure $CuPbSbS_3$. The phase evolution of bulk, drop-cast films of $CuPbSbS_3$ was tracked by ex situ powder XRD as a function of time and temperature (**Figure S1**). At low temperatures and early times (i.e., 330 °C, 30 min) the predominant phases present were binary PbS and ternary $CuSbS_2$ with a minor fraction of bournonite $CuPbSbS_3$. By increasing the annealing temperature and time (i.e., 450 °C, 12 h), the amount of PbS and $CuSbS_2$ gradually decrease to yield an increasing fraction of $CuPbSbS_3$,

presumably via solid-state reaction ($CuSbS_2$ + PbS → $CuPbSbS_3$). A dark gray material was recovered after annealing the drop-cast dried ink to 450 °C for 96 h, which was confirmed to be phase-pure orthorhombic $CuPbSbS_3$ by powder XRD, as shown in **Figure 3**. Rietveld refinement of the XRD pattern using the $Pmn2_1$ space group gives lattice parameters of a = 7.8158(58), b = 8.1515(17), and c = 8.6729(54) Å, and a unit cell volume of V = 552.5634(34) Å^3. These values are in close agreement with the previously reported values for synthetic bulk bournonite (i.e., a = 7.810, b = 8.150, and c = 8.701 Å; V = 553.85 Å^3).[12]

As seen with quaternary chalcogenides, such as kesterite and stannite, X-ray diffraction is not always sufficient to assess phase purity of thin film samples.[34,35] Therefore, Raman spectroscopy was also used to evaluate the phase purity of our $CuPbSbS_3$ thin films (**Figure S2**). Using a 785 nm excitation wavelength, Raman bands corresponding to bournonite Sb-S bending modes were observed at 332 cm^{-1} and 297 cm^{-1} and a lattice mode at 198 cm^{-1} that match well with a naturally occurring single crystal sample.[36] Thin films of $CuSbS_2$ have Raman active modes at ca. 250 cm^{-1} and 350 cm^{-1} and thin films of PbS have Raman active modes at 161 cm^{-1} and 263 cm^{-1}.[37-39] The absence of $CuSbS_2$ and PbS Raman active modes further supports the phase purity of our $CuPbSbS_3$ thin films.

With antimony being present in the largest excess in the ink formulation that returns phase-pure $CuPbSbS_3$, it is likely volatilized during annealing as Sb_2S_3, as has been observed with other multinary antimony-containing sulfides.[40] Inductively coupled plasma optical emission spectroscopy (ICP-OES) was used to quantify the elemental composition of the resulting phase-pure, solution-deposited bournonite. An elemental stoichiometry of $Cu_{1.03}Pb_{1.05}Sb_{1.00}S_3$ was calculated from an average of four analyses. The pseudo-binary PbS–$CuSbS_2$ phase diagram allows for non-stoichiometry in the range of 46-52 mol% PbS in bournonite, which is within the experimental stoichiometry of our material.[41] X-ray photoelectron spectroscopy (XPS) was used to gain information on the valence states of ions in the $CuPbSbS_3$ thin films. A survey scan of a $CuPbSbS_3$ thin film on Si/SiO_2 that had been exposed to ambient conditions is provided in the Supporting Information (**Figure S3**). The high-resolution spectra and corresponding peak fittings for the Cu 2*p*, Pb 4*f*, Sb 3*d*, and S 2*p* regions are given in **Figure S5a**-**S8a**, respectively, and the fitted peak positions and peak splitting values for each high-resolution spectrum are given in **Table S2**. The Cu 2*p* region can be fit with a single doublet of peaks centered at 951.3 eV and 931.5 eV that indicates a single Cu^+ environment for copper in the material. This is consistent with the peak splitting and binding energies for Cu^+ in other quaternary chalcogenides.[26,40] The lack of strong satellites suggests that there is no significant amount of Cu^{2+} in the material, indicating that Cu^{2+} in the solid CuO precursor is reduced to Cu^+ upon dissolution and annealing.[26,42,43] The Pb 4*f* region can be fit with two sets of doublets, each with a splitting of ~4.8 eV. The observation of two different lead environments has been similarly reported for PbS,[44,45] with the higher binding energy doublet for $CuPbSbS_3$ (centered at 143.0 and 138.1 eV) being attributed to oxidized lead species (PbO_x) on the surface and the lower binding energy doublet (centered at 142.7 and 137.9 eV) being attributed to Pb^{2+} in a sulfide environment. Likewise, the Sb 3*d* region can be fit with two sets of doublets, each with a splitting of ~9.3 eV. The observation of two distinct environments for antimony has previously been observed in bulk Sb_2S_3 thin films;[46] here, the appearance of a doublet centered at 539.5 and 529.9 eV is associated with Sb_xO_y surface species and the doublet centered at 538.3 and 529.0 eV is assigned to Sb^{3+} in a sulfide environment. In the S 2*p* region, a doublet and a singlet can be deconvoluted from the high-resolution spectrum. The doublet has a splitting of 1.1 eV which is attributed to the $2p_{1/2}$ and $2p_{3/2}$ of S^{2-} and a broad singlet centered at 163.1 eV assigned to surface oxidation (i.e., SO_x).[42] Thus, XPS analysis verifies the valence states in the material to be $Cu^+Pb^{2+}Sb^{3+}(S^{2-})_3$ with evidence for surface oxides. The observation of surface oxides can be corroborated with the appearance of an O 1*s* peak in the survey scan. It is reasonable to observe surface oxides by XPS since our solution-deposited $CuPbSbS_3$ was not kept in an air-free environment after annealing and amorphous oxides would not be observed by XRD. To determine the extent of oxides present in our thin films, an in situ Ar^+ ion beam treatment was done for 5 min to etch away a few nanometers of the thin film surface. A survey spectrum of the etched thin film is provided in **Figure S4.** As can be seen by the Cu 2*p*, Pb 4*f*, Sb 3*d*, and S 2*p* regions in **Figures S5b**-**S8b**, respectively, only slight reductions in oxidic peaks are observed, which suggests oxide impurities may be persistent throughout the thin film using these processing conditions (fitted peak positions and peak splitting values are given in **Table S3**).

To extend the versatility of the thiol-amine solvent system, a natural mineral sample of bournonite mined from Chihuahua, Mexico was obtained from the Natural History Museum of Los Angeles. A ground sample of the natural mineral appeared phase pure by powder XRD (**Figure S9**). An ink containing 60 mg mL^{-1} of the natural bournonite sample was fully dissolved in a 1:4 (vol/vol) mixture of EDT and en, respectively, at room temperature over 12 h. The resulting ink is an optically clear and free-flowing orange-brown solution that is qualitatively identical to the synthetic ink derived from the dissolution of CuO, PbO, and Sb_2S_3 (**Figure S10**). Drop-cast bulk films of the dried ink were annealed at 450 °C for 96 h under conditions identical to those used for the synthetic ink. Interestingly, this returned crystalline $CuPbSbS_3$ with a significant PbS impurity (**Figure S11**). Taken with the existing literature on synthetic bulk $CuPbSbS_3$,[14] this result reinforces the difficulty of isolating phase-pure bournonite even when starting from a seemingly phase-pure naturally occurring mineral. This highlights the versatility of the thiol-amine solvent system to fine tune synthetic ink compositions for the recovery of phase-pure multinary chalcogenides by easily tuning the ratios of the bulk binary ink constituents.

Thin Film Deposition. To demonstrate the utility of the alkahest to give high-quality thin films, a 2× concentrated ink

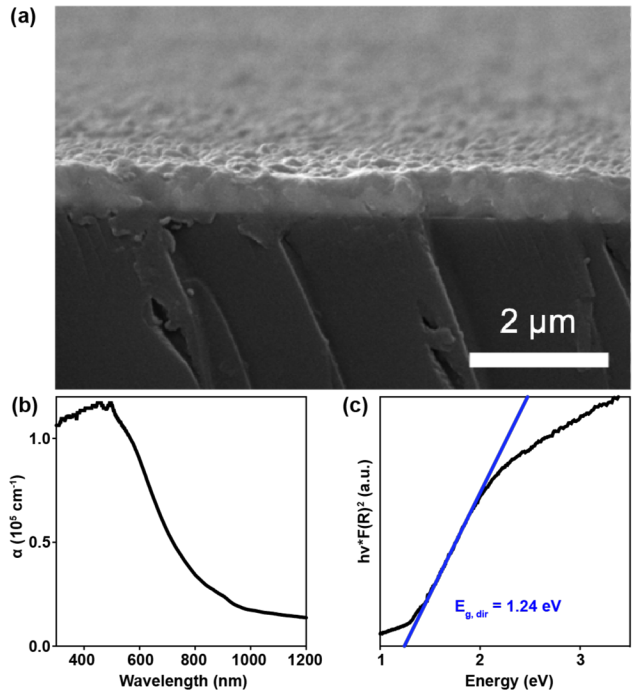

Figure 4. (a) Cross-sectional SEM micrograph of a $CuPbSbS_3$ thin film deposited on a borosilicate glass substrate. (b) Plot of absorption coefficient (α) as a function of wavelength, and (c) Tauc plot extrapolated to estimate a direct optical band gap of 1.24 eV.

(120 mg/mL) was used to solution deposit 3 coats onto a glass substrate via spin coating at 3000 rpm for 1 min with annealing to 390 °C between coats and a final anneal to 450 °C for 20 min.

While phase-pure $CuPbSbS_3$ thin films can be obtained by annealing to 390 °C for 10 min, improved grain density in the thin films was achieved by annealing to 450 °C for 20 min (**Figure 4a** and **S12**). Phase-pure $CuPbSbS_3$ thin films are obtained at lower temperatures than the bulk, drop cast films (i.e., 450 °C, 96 h for bulk, drop cast films *vs* 390 °C, 10 min for spin coated thin films). The differences in annealing times between bulk and thin films can be explained by solid-state diffusion in a thin film proceeding more readily than in a bulk powder. In the bulk, solid-state diffusion is limiting, whereas for thin films the formation of the desired phase is nucleation limited.[47] If the thin films are annealed at 450 °C for extended times (i.e., > 60 min), PbS and $CuSbS_2$ impurity phases begin to appear, suggesting that the $CuPbSbS_3$ thin film disproportionates at high temperatures and extended annealing times. Solution deposition results in specularly reflective thin films of $CuPbSbS_3$ that are dark gray in color and free from imperfections (i.e., pin holes, microcracks, edge effects, striations). Cross-sectional scanning electron microcopy (SEM) was used to assess film thickness. The resulting thin films possessed an average thickness of 565 nm.

Property Measurements. The absorption coefficient and optical band gap of the resulting $CuPbSbS_3$ was measured by UV-vis-NIR spectroscopy. An absorption spectrum derived from transmittance data and the optical band gap from recovered powder using an integrating sphere are provided in **Figure 4b** and **4c**, respectively. An absorption coefficient of $\alpha = 3.0 \times 10^4$ cm^{-1} at 826 nm (1.5 eV) rises to $\alpha = 1.1 \times 10^5$ cm^{-1} at 516 nm (2.4 eV) for a 570 nm thick thin film. A direct optical band gap of $E_{g,dir}$ = 1.24 eV was determined after extrapolating the square of the linear portion of the diffuse reflectance spectrum (**Figure 4c**); this band gap lies within the range of previously reported experimental values for bournonite (ca. 1.20 eV to 1.31 eV)[11,12] and is slightly lower than the theoretically predicted value (1.41 eV)[8].

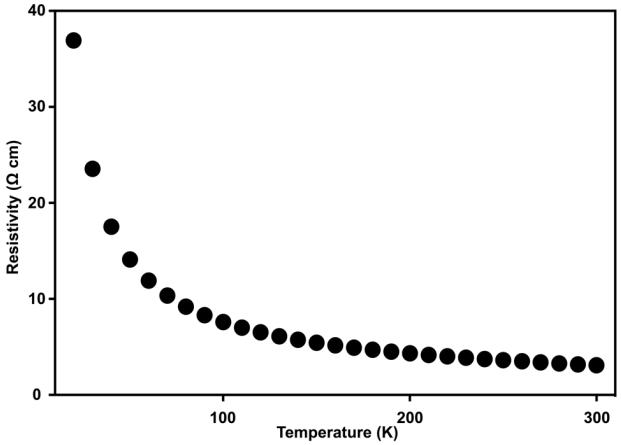

Figure 5. Resistivity (ρ) of a $CuPbSbS_3$ thin film as a function of temperature.

There is a single report on the Hall coefficient of a single crystal of bournonite collected in the range from 277-833 K,[11] but the electronic properties of phase-pure thin films of bournonite have not been explored. The electronic transport properties of the resulting $CuPbSbS_3$ thin films were studied using the Van der Pauw geometry, with measurements performed in a physical property measurement system (PPMS). Measurements were conducted in the temperature range of 10-300 K, with the resistivity as a function of temperature behaving like a typical intrinsic semiconductor where the resistivity increases drastically at low temperatures (**Figures 5**, **S14**). Depending on the film, ranging in average thickness from 562-570 nm, carrier concentrations were found to be between 6.2×10^{18} – 3.5×10^{20} cm^{-3} with the associated carrier mobilities ranging from 0.01-2.4 cm^2 (V•s)$^{-1}$. These values are in the lower range of previously reported values for solution processed hybrid lead iodide perovskite thin films (e.g., 0.2–71 cm^2 (V•s)$^{-1}$),[48] but are consistent with $CuPbSbS_3$ being a heavily doped *p*-type semiconductor. Hall measurements and the majority carrier type are very sensitive to the processing conditions. Since the thin films were deposited on insulating borosilicate glass, the electrical properties may ultimately differ from those deposited on conducting substrates in a photovoltaic device architecture with respect to impurities and grain size. Natural samples of bournonite have been reported to have *n*-type conductivity but density functional theory calculations suggest *n*-type behavior in $CuPbSbS_3$ to be highly unlikely.[13,50] The high carrier concentrations observed here may be due to small off-stoichiometry in the solution-processed films or oxidic defects, as evidenced by XPS (vide supra).

Carrier concentrations of solution processed and vacuum deposited quaternary $Cu_2ZnSn(S,Se)_4$ semiconductors have shown carrier concentrations ranging from 10^{17} – 10^{19} cm^{-3} attributed to differences in grain structures/boundaries and incorporated impurities, with carrier concentrations reported as high as 3.1×10^{20} cm^{-3}.[34,35]

To further evaluate the potential use of this material for solar energy conversion, the transient photoresponse of a $CuPbSbS_3$ thin film device was tested. The $CuPbSbS_3$ absorber layer was spin coated on a patterned fluorine-doped SnO_2 (FTO) substrate with a lateral spacing of ~20 μm. The device was exposed to chopped white light with an AM1.5G filtered 300 W xenon arc lamp under ambient conditions and yielded a photoresponse of >225 nA at a potential of -500 mV (**Figure S15**). The electronic properties of our thin films, combined with their high absorption coefficient, and near-optimal direct band gap suggest that $CuPbSbS_3$ deposited with this thiol-amine method may yield suitable absorber layers for photovoltaic devices given the proper deposition conditions and device architecture.[49]

CONCLUSIONS

In summary, we have demonstrated the ability of our alkahest solvent system to solution process high-quality thin films of bournonite $CuPbSbS_3$ under mild conditions from an ink comprised of dissolved bulk CuO, PbO, and Sb_2S_3 in EDT and en. Having the ability to fine tune the compound ink composition by simply adjusting the stoichiometry of the bulk precursors allows for the deposition of phase-pure $CuPbSbS_3$. While the same thiol-amine solvent mixture is capable of dissolving naturally occurring bournonite, this ink returns $CuPbSbS_3$ with PbS impurities similar to previously reported solid-state syntheses.

The resulting $CuPbSbS_3$ thin films possess a direct optical band gap of 1.24 eV and a high absorption coefficient in the visible range of ~10^5 cm^{-1}. Electronic measurements confirm that the solution-processed $CuPbSbS_3$ thin film has mobilities in the range of 0.01-2.4 cm^2 $(V\bullet s)^{-1}$ and carrier concentrations of 10^{18} –10^{20} cm^{-3}. This highlights the potential use of bournonite as an absorber layer in thin film solar cells and demands further study.

This method should be generalizable to the solution deposition of other multinary semiconductor thin films, including compositionally related I-IV-V-VI_2 semiconductors such as $CuPbBiS_3$. Aikinite $CuPbBiS_3$ is another naturally occurring sulfosalt mineral that has recently been identified through the screening of ~800 materials from the Materials Project Database for favorable properties for potential photovoltaic absorbers.[51] Indeed, preliminary results show that the same thiol-amine solvent mixture is capable of dissolving a mixture of bulk CuO, PbO, and Bi_2S_3 precursors. This unoptimized compound ink returned a mixture of the desired crystalline $CuPbBiS_3$ phase (*Pnma*) with a slight PbS impurity upon annealing at 450 °C for 48 h (**Figure S16**). These combined results highlight the promise of the alkahest method for the solution deposition of sulfosalt absorber layers for photovoltaics.

ASSOCIATED CONTENT

Supporting Information

The Supporting Information is available free of charge on the ACS Publications website.

Additional experimental details, photographs comparing ink compositions, structural parameters from Rietveld refinement, Raman spectrum, variable temperature XRD patterns, XPS spectra, cross-sectional SEM micrograph of film annealed to 390 °C, transmittance spectrum of $CuPbSbS_3$ thin film, photographs of $CuPbSbS_3$ mineral sample, XRD patterns of $CuPbSbS_3$ mineral before and after dissolution and recovery (PDF), resistivity data, photoconductivity data, XRD pattern of $CuPbBiS_3$ (PDF)

AUTHOR INFORMATION

Corresponding Author

* brutchey@usc.edu

ACKNOWLEDGMENTS

RLB acknowledges support from the National Science Foundation under DMR-1904719. We thank B. Tappan, J. Milam-Guerrero, J. Intrator, A. Tadle and Dr. E. Roberts for help with data collection and analysis.

REFERENCES

(1) Haegel, N. M.; Margolis, R.; Buonassisi, T.; Feldman, D.; Froitzheim, A.; Garabedian, R.; Green, M.; Glunz, S.; Henning, H.-M.; Holder, B.; Kaizuka, I.; Kroposki, B.; Matsubara, K.; Niki, S.; Sakurai, K.; Schindler, R. A.; Tumas, W.; Weber, E. R.; Wilson, G.; Woodhouse, M.; Kurtz, S. Terawatt-Scale Photovoltaics: Trajectories and Challenges. *Science* **2017**, *356*, 141–143.

(2) Shin, S. S.; Yeom, E. J.; Yang, W. S.; Hur, S.; Kim, M. G.; Im, J.; Seo, J.; Noh, J. H.; Seok, S. I. Colloidally Prepared La-Doped $BaSnO_3$ Electrodes for Efficient, Photostable Perovskite Solar Cells. *Science* **2017**, *356*, 167–171.

(3) Green, M. A.; Ho-Baillie, A.; Snaith, H. J. The Emergence of Perovskite Solar Cells. *Nat. Photonics* **2014**, *8*, 506–514.

(4) Stranks, S. D.; Eperon, G. E.; Grancini, G.; Menelaou, C.; Alcocer, M. J. P.; Leijtens, T.; Herz, L. M.; Petrozza, A.; Snaith, H. J. Electron-Hole Diffusion Lengths Exceeding 1 Micrometer in an Organometal Trihalide Perovskite Absorber. *Science* **2013**, *342*, 341–344.

(5) Dong, Q.; Fang, Y.; Shao, Y.; Mulligan, P.; Qiu, J.; Cao L.; Huang, J. Electron-Hole Diffusion Lengths > 175 μm in Solution-Grown $CH_3NH_3PbI_3$ Single Crystals. *Science* **2015**, *347*, 967–970.

(6) Frost, J. M.; Butler, K. T.; Brivio, F.; Hendon, C. H.; van Schilfgaarde, M.; Walsh, A. Atomistic Origins of High-Performance in Hybrid Halide Perovskite Solar Cells. *Nano Lett.* **2014**, *14*, 2584–2590.

(7) Song, Z.; Abate, A.; Watthage, S. C.; Liyanage, G. K.; Phillips, A. B.; Steiner, U.; Graetzel, M.; Heben, M. J. Perovskite Solar Cell Stability in Humid Air: Partially Reversible Phase Transitions in the PbI_2-CH_3NH_3I-H_2O System. *Adv. Energy Mater.* **2016**, *6*, 1600846.

(8) Wallace, S. K.; Svane, K.; Huhn, W. P.; Zhu, T.; Mitzi, D. B.; Blum, V.; Walsh, A. Candidate Photoferroic Absorber Materials for Thin-Film Solar Cells from Naturally Occurring Minerals: Enargite, Stephanite, and Bournonite. *Sustain. Energy Fuels* **2017**, *1*, 1339–1350.

(9) Ganose, A. M.; Savory, C. N.; Scanlon, D. O. Beyond Methylammonium Lead Iodide: Prospects for the Emergent Field of ns2 Containing Solar Absorbers. *Chem. Commun.* **2017**, *53*, 20–44.

(10) Yu, L.; Zunger, A. Identification of Potential Photovoltaic Absorbers Based on First-Principles Spectroscopic Screening of Materials. *Phys. Rev. Lett.* **2012**, *108*, 068701.

(11) Bairamova, S. T.; Bagieva, M. R.; Agapashaeva, S. M.; Aliev, O. M. Synthesis and Properties of Structural Analogs of the Mineral Bournonite. *Inorg. Mater*. **2011**, *47*, 345–348.

(12) Wei, K.; Martin, J.; Salvador, J. R.; Nolas, G. S. Synthesis and Characterization of Bournonite $PbCuSbS_3$ Nanocrystals. *Cryst. Growth Des.* **2015**, *15*, 3762–3766.

(13) Durant, B.; Parkinson, B. A. Photovoltaic Response of Naturally Occurring Semiconducting Sulfide Minerals. *2016 IEEE 43rd Photovoltaic Specialists Conference*; IEEE: New York, 2016; pp 2774-2779.

(14) Dong, Y.; Khabibullin, A. R.; Wei, K.; Salvador, J. R.; Nolas, G. S.; Woods, L. M. Bournonite $PbCuSbS_3$: Stereochemically Active Lone-Pair Electrons that Induce Low Thermal Conductivity. *ChemPhysChem* **2015**, *16*, 3264–3270.

(15) Frumar, M.; Kala, T.; Horak, J. Growth and Some Physical Properties of Semiconducting $CuPbSbS_3$ Crystals. *J. Cryst. Growth* **1973**, *20*, 239–244.

(16) Eslamian, M. Inorganic and Organic Solution-Processed Thin Film Devices. *Nano-Micro Lett.* **2017**, *9*, 3.

(17) Mitzi, D. B. Solution-Processed Inorganic Semiconductors. *J. Mater. Chem.* **2004**, *14*, 2355-2365.

(18) Mitzi, D. B.; Kosbar, L. L.; Murray, C. E.; Copel, M.; Afzali, A. High-Mobility Ultrathin Semiconducting Films Prepared by Spin Coating. *Nature* **2004**, *428*, 299-303.

(19) Mitzi, D. B.; Yuan, M.; Liu, W.; Kellock, A. J.; Chey, S. J.; Deline, V.; Schrott, A. G. A High-Efficiency Solution-Deposited Thin-Film Photovoltaic Device. *Adv. Mater*. **2008**, *20*, 3657-3662.

(20) Mitzi, D. B. Solution Processing of Chalcogenide Semiconductors via Dimensional Reduction. *Adv. Mater*. **2009**, *21*, 3141-3158.

(21) Webber, D. H.; Brutchey, R. L. Alkahest for V_2VI_3 Chalcogenides: Dissolution of Nine Bulk Semiconductors in a Diamine-Dithiol Solvent Mixture. *J. Am. Chem. Soc*. **2013**, *135*, 15722−15725.

(22) Webber, D. H.; Buckley, J. J.; Antunez, P. D.; Brutchey, R. L. Facile Dissolution of Selenium and Tellurium in a Thiol–amine Solvent Mixture under Ambient Conditions. *Chem. Sci*. **2014**, *5*, 2498–2502.

(23) Antunez, P. D.; Torelli, D. A.; Yang, F.; Rabuffetti, F. A.; Lewis, N. S.; Brutchey, R. L. Low Temperature Solution-Phase Deposition of SnS Thin Films. *Chem. Mater.* **2014**, *26*, 5444−5446.

(24) McCarthy, C. L.; Webber, D. H.; Schueller, E. C.; Brutchey, R. L. Solution-Phase Conversion of Bulk Metal Oxides to Metal Chalcogenides Using a Simple Thiol–Amine Solvent Mixture. *Angew. Chem., Int. Ed.* **2015**, *54*, 8378−8381.

(25) McCarthy, C. L.; Cottingham, P.; Abuyen, K.; Schueller, E. C.; Culver, S. P.; Brutchey, R. L. Earth Abundant $CuSbS_2$ Thin Films Solution Processed from Thiol–Amine Mixtures. *J. Mater. Chem. C* **2016,** *4*, 6230−6233.

(26) McCarthy, C. L.; Brutchey, R. L. Solution Deposited $Cu_2BaSnS_{4-x}Se_x$ from a Thiol–Amine Solvent Mixture. *Chem. Mater.* **2018**, *30*, 304−308.

(27) McCarthy, C. L.; Brutchey, R. L. Solution Processing of Chalcogenide Materials Using Thiol–Amine "Alkahest" Solvent Systems. *Chem. Commun.* **2017**, *53*, 4888−4902.

(28) Zhao, X.; Lu, M.; Koeper, M. J.; Agrawal, R. Solution-Processed Sulfur Depleted $Cu(In,Ga)Se_2$ Solar Cells Synthesized from a Monoamine-Dithiol Solvent Mixture. *J. Mater. Chem. A* **2016**, *4*, 7390-7397.

(29) Yang, Y.; Wang, G.; Zhao, W.; Tian, Q.; Huang, L.; Pan, D. Solution-Processed Highly Efficient $Cu_2ZnSnSe_4$ Thin Film Solar Cells by Dissolution of Elemental Cu, Zn, Sn, and Se Powders. *ACS Appl. Mater. Interfaces* **2015**, *7*, 460-464.

(30) Arnou, P.; van Hest M. F. A. M.; Cooper, C. S.; Malkov, A. V.; Walls, J. M.; Bowers, J. W. Hydrazine-Free Solution-Deposited $CuIn(S,Se)_2$ Solar Cells by Spray Deposition of Metal Chalcogenides. *ACS Appl. Mater. Interfaces* **2016**, *8*, 11893-11897.

(31) Dittrich, A.; Bieniok, A.; Brendel, U.; Grodzicki, M.; Topa, D. Sulfosalts – A New Class of Compound Semiconductors for Photovoltaic Applications. *Thin Solid Films* **2007**, *515*, 5745-5750.

(32) Buckley, J. J.; McCarthy, C. L.; Pilar-Albaladejo, J. D.; Rasul, G.; Brutchey, R. L. Dissolution of Sn, SnO, SnS in a Thiol-Amine Solvent Mixture: Insights into the Identity of the Molecular Solutes for Solution-Processed SnS. *Inorg. Chem.* **2016**, *55*, 3175-3180.

(33) Hayashi, M.; Shiro, Y.; Oshima, T.; Murata, H. The Vibrational Assignment, Rotational Isomerism and Force Constants of 1,2-Ethanedithiol. *Bull. Chem. Soc. Jpn*. **1965**, *38*, 1734−1740.

(34) Mitzi, D. B.; Gunawan, O.; Todorov, T. K.; Wang, K.; Guha, S. The Path Towards a High-Performance Solution-Processed Kesterite Solar Cell. *Sol. Energy Mater. Sol. Cells* **2011**, *95*, 1421−1436.

(35) Chen, S.; Walsh, A.; Gong, X. G.; Wei, S. H. Classification of Lattice Defects in the Kesterite Cu_2ZnSnS_4 and $Cu_2ZnSnSe_4$ Earth-Abundant Solar Cell Absorbers. *Adv. Mater.* **2013**, *25*, 1522-1539.

(36) Kharbish, S.; Libowitzky, E.; Beran, A. Raman Spectra of Isolated and Interconnnected Pyramidal XS_3 Groups (X = Sb, Bi) in Stibnite, Bismuthinite, Kermesite, Stephanite and Bournonite. *Eur. J. Mineral* **2009**, *21*, 325-333.

(37) Baker, J.; Kumar, R. S.; Sneed, D.; Connolly, A.; Zhang, Y.; Velisavljevic, N.; Paladugu, J.; Pravica, M.; Chen, C.; Cornelius, A.; Zhao, Y. Pressure Induced Structural Transitions in $CuSbS_2$ and $CuSbSe_2$ Thermoelectric Compounds. *J. Alloys Compd.* **2015**, *643*, 186− 194.

(38) Thiruvenkadam, S.; Rajesh, A. L. Effect of Temperature on Structural and Optical Properties of Spray Pyrolysed $CuSbS_2$ Thin Films for Photovoltaic Applications. *Int. J. Sci. Eng. Res.* **2014**, *5*, 248-251.

(39) Rajashree, C.; Balu, A. R. Tuning the Physical Properties of PbS Thin Films Towards Optoelectronic Applications Through Ni Doping. *Optik* **2016**, *127*, 8892-8898.

(40) McClary, S. A.; Balow, R. B.; Argawal, R. Role of Annealing Atmosphere on the Crystal Structure and Composition of Tetrahedrite-Tennantite Alloy Nanoparticles. *J. Mater. Chem. C.* **2018**, *6*, 10538-10546.

(41) Aliyev, O. M.; Ajdarova, D. S.; Bayramova, S. T.; Aliyeva, S. I.; Ragimova, V. M. Nonstoichiometry in $PbCuSbS_3$ Compound. *Azerbaijan Chem. J.* **2016**, *2*, 51-54.

(42) Ge, J.; Yan, Y. Synthesis and Characterization of Photoelectrochemical and Photovoltaic Cu_2BaSnS_4 Thin Films and Solar Cells. *J. Mater. Chem. C* **2017**, *5*, 6406−6419.

(43) Moulder, J. F.; Stickle, W. F.; Sobol, P. E.; Bomben, K. D. Handbook of X-Ray Photoelectron Spectroscopy; Chastain, J., Ed.; Physical Electronics Division, *Perkin-Elmer Corp.*: Eden Prairie, MN, **1979**.

(44) Hardman, S. J. O.; Graham, D. M.; Stubbs, S. K.; Spencer, B. F.; Seddon, E. A.; Fung, H. T.; Gardonio, S.; Sirotti, F.; Silly, M. G.; Akhtar, J.; O'Brien, P.; Binks, D. J.; Flavell, W. R. Electronic and Surface Properties of PbS Nanoparticles Exhibiting Efficient Multiple Exciton Generation. *Phys. Chem. Chem. Phys.* **2011**, *13*, 20275−20283.

(45) Cant, D. J. H.; Syres, K. L.; Lunt, P. J. B.; Radtke, H.; Treacy, J.; Thomas, P. J.; Lewis, E. A.; Haigh, S. J.; O'Brien, P.; Schulte, K.; Bondino, F.; Magnano, E.; Flavell, W. R.; Surface Properties of Nanocrystalline PbS Films Deposited at the Water−Oil Interface: A Study of Atmospheric Aging. *Langmuir* **2015**, *31*, 1445-1453.

(46) Godel, K. C.; Roose, B.; Sadhanala, A.; Vaynzof, Y.; Pathak, S. K.; Steiner, U. Partial Oxidation of the Absorber Layer Reduces Charge Carrier Recombination in Antimony Sulfide Solar Cells. *Phys. Chem. Chem. Phys.* **2017**, *19*, 1425.

(47) Novet, T.; Johnson, D. C. New Synthetic Approach to Extended Solids: Selective Synthesis of Iron Silicides via the Amorphous State. *J. Am. Chem. Soc.* **1991**, *113*, 3398–3403.

(48) Herz, L. M. Charge-Carrier Mobilities in Metal Halide Perovskites: Fundamental Mechanisms and Limits. *ACS Energy Lett.* **2017**, *2*, 1539–1548.

(49) Wallace, S. K.; Butler, K. T.; Hinuma, Y.; Walsh, A. Finding a Junction Partner for Candidate Solar Cell Absorbers Enargite and Bournonite from Electronic Band and Lattice Matching. *J. Appl. Phys.* **2019**, *125*, 055703.

(50) Faghaninia, A.; Guodong, Y.; Aydemir, U.; Wood, M.; Chen, W.; Rignanese, G.-M.; Snyder, G. J.; Hautier, G.; Jain, A. A Computational Assessment of the Electronic, Thermoelectric, and Defect Properties of Bournonite ($CuPbSbS_3$) and Related Substitutions. *Phys. Chem. Chem. Phys.*, **2017**, *19*, 6743-6756.

(51) Fabini, D. H.; Koerner, M.; Seshadri, R. Candidate Inorganic Photovoltaic Materials from Electronic Structure-Based Optical Absorption and Charge Transport Proxies. *Chem. Mater.* **2019**, *31*, 1561–1574.

Authors are required to submit a graphic entry for the Table of Contents (TOC) that, in conjunction with the manuscript title, should give the reader a representative idea of one of the following: A key structure, reaction, equation, concept, or theorem, etc., that is discussed in the manuscript. Consult the journal's Instructions for Authors for TOC graphic specifications.